SPACE SCIENCES

Specularly reflected whistler: A low-latitude channel to couple lightning energy to the magnetosphere

Vikas S. Sonwalkar[1]* and Amani Reddy[1,2]

Lightning-generated whistlers profoundly affect the energetic particle population in Earth's radiation belts, influencing space weather and endangering astronauts and satellites. We report the discovery of specularly reflected (SR) whistler in which the lightning energy injected into the ionosphere at low latitudes reaches the magnetosphere after undergoing a specular reflection in the conjugate ionosphere, contradicting previous claims that lightning energy injected at low latitudes cannot escape the ionosphere. SR whistlers provide a low-latitude channel to transport lightning energy to the magnetosphere. We calculate the relative contributions of SR, magnetospherically reflected, subprotonospheric, and ducted whistlers to the lightning energy reaching the magnetosphere. When SR whistlers are considered, the global lightning energy contribution to the magnetosphere doubles, implying that the previous estimates of the impact of lightning energy on radiation belts may need substantial revisions. Whistler dispersion and intensity analyses quantitatively confirm our results and suggest new remote-sensing methods of the magnetosphere, ionosphere, Earth-ionosphere waveguide, and lightning flashes.

INTRODUCTION

The lightning energy injected into the Earth's magnetosphere propagates as a whistler, a highly dispersed form of electromagnetic energy (*1*–*5*). Whistlers play an important role in the physics of radiation belts, contributing to the precipitation of energetic particles (*6*–*11*), generation of hiss (*12*–*16*), and formation of slot region (*10*, *11*, *17*, *18*). Whistlers are a powerful tool for remote sensing magnetospheric plasma (*1*, *4*, *19*–*22*).

The whistlers, typically observed in the ~100-Hz to 10-kHz frequency range, are categorized as ducted or nonducted whistlers. Ducted whistlers propagating at small wave normal angles in field-aligned ducts of enhanced or decreased ionization are observable on the ground (*4*) and spacecraft (*5*). Nonducted whistlers propagating at relatively large wave normal angles and crossing magnetic field lines are observable only on satellites before (directly) or after one or more reflections within the magnetosphere; they are called magnetospherically reflected (MR) whistlers (*5*, *21*, *23*, *24*). Another type of nonducted whistler, called subprotonospheric (SP) whistler, undergoes reflections below ~1000-km altitude and is confined to the ionosphere (*3*, *25*–*27*).

This paper reports the discovery of specularly reflected (SR) whistler in which the lightning energy injected at low latitudes is first specularly reflected at the Earth-ionosphere (E-I) boundary in the conjugate hemisphere, and then it propagates upward to the magnetosphere (*28*). SR whistlers carry lightning energy injected at lower latitudes to the magnetosphere, whereas MR whistlers carry that injected at higher latitudes to the magnetosphere. SR and MR whistlers are distinct phenomena that coexist in the magnetosphere. Our results contradict those of previous works (*18*, *29*), claiming that the lightning energy injected at low latitudes cannot escape the ionosphere. When we consider SR whistlers, the total global lightning energy contribution to the magnetosphere doubles, implying that the previous estimates of the impact of lightning energy on radiation belts need substantial revisions.

The paper presents SR whistler observations and occurrence patterns, ray tracing interpretation, estimates of relative lightning energy contributions to the magnetosphere by SR, MR, SP, and ducted whistlers and a discussion of the impact of SR whistlers on radiation belts and their potential for remote sensing of the magnetosphere, ionosphere, and lightning.

RESULTS

Observations and interpretation

The data reported here were obtained by the Electric and Magnetic Field Instrument Suite and Integrated Science (EMFISIS) on Van Allen Probes, previously called Radiation Belt Storm Probes (RBSP) and comprised of RBSP-A and RBSP-B satellites (see Materials and Methods, "Instrumentation, datasets, and data analysis methods" section) (*30*–*32*). Figure 1A (fig. S1) shows the spectrogram of three sets of multicomponent SR and MR whistlers received by the B_w antenna of the waveform receiver (WFR) on the RBSP-A satellite. Each set of multicomponent whistlers resulted from a single lightning flash. Consider the set 2 whistlers, generated by the lightning flash at time L2 (black arrow) and observed from about ~1 s onward with 0_+^{MR} as the first component. Each whistler in the set, indicated by cyan, blue, or red arrow, is characterized by a lower and an upper cutoff frequency and a distinctive dispersion, t_g-f, where t_g is the signal group time delay from the source lightning to RBSP-A at frequency f. Figure 1 (B and C) provides a qualitative interpretation of the observed whistlers and help understand their nomenclature, as discussed below. A broadband impulsive signal from lightning illuminates the E-I boundary (assumed at 90 km here) over a range of latitudes and longitudes. Some of the lightning energy injected into the ionosphere in the magnetic meridional plane of RBSP-A reaches it by several distinct nonducted ray paths and is observed as set 2 whistlers (Fig. 1A). As illustrated in Fig. 1 (B and C), the energy injected at higher latitudes reaches the satellite directly by a nonducted ray path and produces an 0_+^{MR} whistler (cyan ray); the energy

[1]Department of Electrical Engineering, University of Alaska Fairbanks, Fairbanks, AK 99709, USA. [2]Geophysical Institute, University of Alaska Fairbanks, Fairbanks, AK 99709, USA.
*Corresponding author. Email: vssonwalkar@alaska.edu

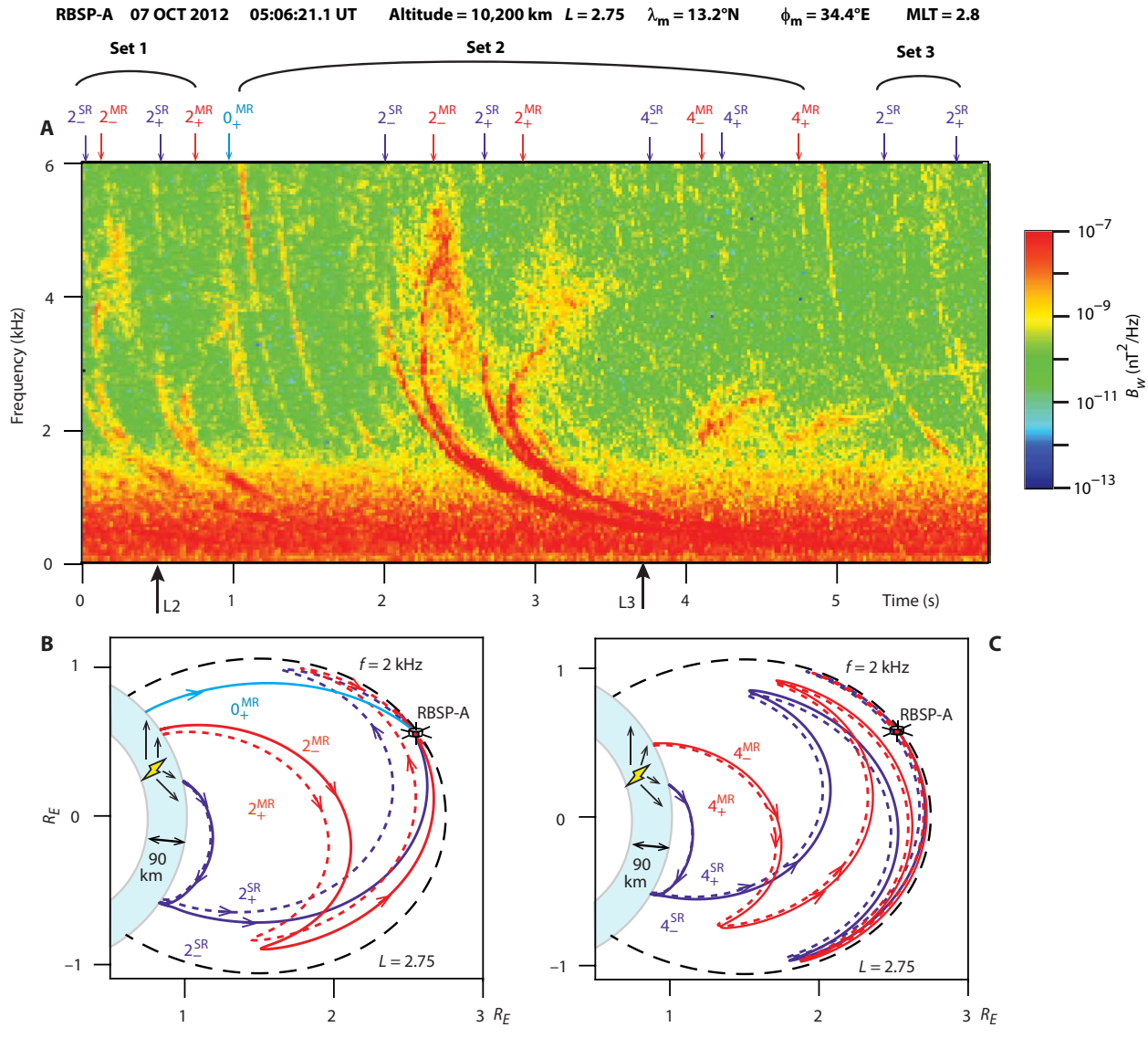

Fig. 1. Observations and interpretation of SR and MR whistlers. (**A**) Spectrogram showing direct nonducted (0^{MR}_{+}; cyan arrow), MR (2^{MR}_{-}, 2^{MR}_{+}, …; red arrows), and SR (2^{SR}_{-}, 2^{SR}_{+}, …; blue arrows) whistlers observed on the RBSP-A satellite. The satellite location in McIlwain *L* parameter (*L*), geomagnetic latitude (λ_m), geomagnetic longitude (ϕ_m), and magnetic local time (MLT) is given at the top. Multicomponent whistlers in set 1, set 2, and set 3 are generated by lightning flashes L1 (not shown), L2, and L3, respectively, indicated by black arrows. The lightning flash L1 corresponding to set 1 whistlers occurred at the time of −1.65 s and at $\lambda_m = 20.8°$N, $\phi_m = 36.8°$E. (**B** and **C**) Ray paths of various whistler components showing the propagation of lightning energy at 2 kHz from its source location (indicated by the yellow lightning symbol) to the RBSP-A satellite. The blue shaded region is the E-I waveguide. The dipole field line at $L = 2.75$ (black dashed curve) passing through the satellite is shown for reference. The E-I waveguide is not drawn to scale, but the region above it and ray propagation paths are drawn to scale.

injected at intermediate latitudes undergoes one or more magnetospheric reflections and then produces MR whistlers (red rays); the energy injected at lower latitudes first undergoes a total internal specular reflection at the E-I boundary in the conjugate hemisphere and then propagates upward to produce SR whistlers in the magnetosphere (blue rays). The second and higher reflections of SR whistlers are magnetospheric.

Figure 1 (B and C) shows the ray paths of 2 kHz signals from the lightning to the satellite. Lightning energy at other frequencies, injected at different latitudes but following similar ray paths with varying group velocities, reaches the satellite with differing time delays, producing the spectral forms of various whistlers shown in Fig. 1A. The properties of whistler mode wave propagation in the magnetosphere can explain the broad features of observed lightning-generated SR and MR whistlers, including general spectral shape and cutoff frequencies (see text S1) (*4*, *5*, *21*, *23*, *33*, *34*). Because the propagation path of an SR whistler, after its first specular reflection, is similar to that of an MR whistler, the spectral forms of SR and MR whistlers are similar, as the spectrogram of Fig. 1A shows.

Adapting a nomenclature developed for MR whistlers (*5*), we label each whistler with a numeral (0, 1, 2, …), a subscript "−" or "+"

and a superscript "MR" or "SR." The numeral indicates the number of equatorial crossings of the ray (lightning energy) before it reaches the satellite. The subscript + or − indicates whether or not the ray has undergone a reflection after its last equatorial crossing before it reaches the satellite. The superscript MR or SR refers to the first reflection type—magnetospheric or specular reflection. A whistler that has yet to undergo first reflection (e.g., cyan ray path), a direct whistler, is labeled 0_+ or 1_- and is marked with a superscript MR or SR depending on the type of first reflection the ray would undergo if it were to continue its journey. The labeling of various whistlers shown in Fig. 1A and the associated ray paths shown in Fig. 1 (B and C) illustrate the nomenclature defined above.

Data from the World Wide Lightning Location Network (WWLLN) (*35*) are used to associate causative lightning flashes with whistlers observed on Van Allen Probes (see Materials and Methods, "Instrumentation, datasets, and data analysis methods" section and text S2). The causative lightning flash L1 (not shown in Fig. 1A) of set 1 whistlers was recorded by the WWLLN to have occurred at −1.65 s. Causative lightning flashes L2 and L3 of set 2 and set 3 whistlers were not recorded by the WWLLN, but their times of occurrences were deduced by noting that the corresponding whistlers of set 1, set 2, and set 3 have identical dispersion.

The absence of 0_+ and MR whistlers in set 3 illustrates that MR whistlers do not necessarily accompany SR whistlers. The lack of 0_+ and MR whistlers in set 3 may have resulted from a weak, low-latitude, causative lightning close to SR injection latitudes but distant from 0_+ and MR injection latitudes. Similarly, weak 0_+^{MR} (compared to 2_- and 2_+ whistlers) in set 2 is probably the result of low-latitude causative lightning. The whistlers shown in Fig. 1A were detected on the three electric and three magnetic sensors of the WFR (fig. S2). Intensities of SR and MR whistlers, which have undergone the same number of equatorial crossings and reflections (e.g., $2_-^{SR}$and 2_-^{MR}), on each of the three magnetic (B_u, B_v, and B_w) antennas were comparable, which are consistent with ray tracing predictions of similar wave normal directions for SR and MR whistlers (see next section on ray tracing confirmation) (*36*).

Figure 2 (see also fig. S3) shows another example of a set of SR-MR whistlers originating in a single lightning flash and containing whistlers that have undergone up to six equatorial crossings.

As illustrated in Fig. 3 and fig. S4, SR and MR whistlers often occur in succession over timescales of minutes to tens of minutes along a segment of the satellite orbit covering ~0.1 to 1.0 L-shell range (text S3). Estimated times of causative lightning flash shown by red and blue arrows in these figures were obtained using various

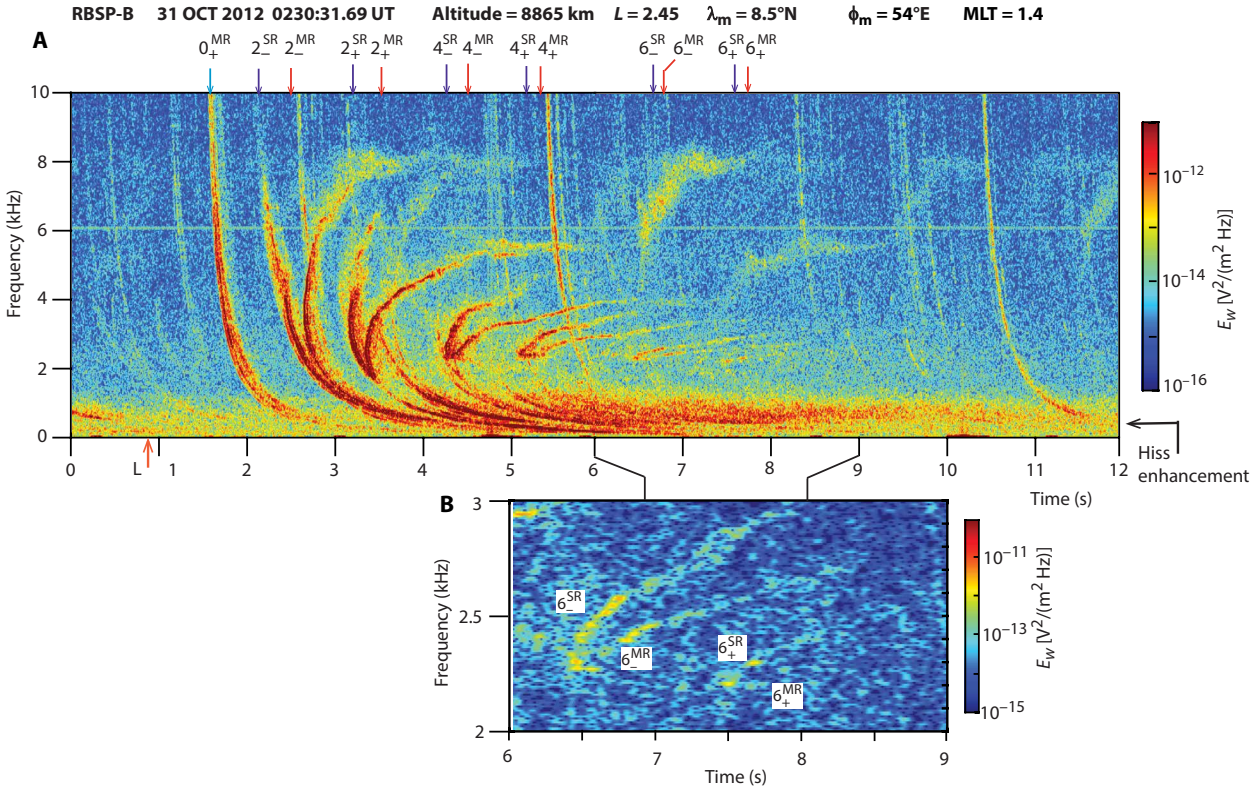

Fig. 2. Example of SR and MR whistlers exhibiting up to 6_- and 6_+ components. (**A**) Spectrum of the E_w component of the electric field observed on the RBSP-B satellite. All six electric and magnetic field antennas detected these whistlers. The causative lightning L, indicated by the red arrow, occurred at the time of 0.95 s and location at $\lambda_m = 29.3°$N, $\phi_m = 52.7°$E, as recorded by the WWLLN. The whistlers produced by this particular lightning flash are labeled. The spectrum also shows several other weak multicomponent SR and MR whistlers produced by other lightning flashes; the 0_+ whistlers of these multicomponent whistlers are easily identifiable at ~2.7, 5.4, 8.3, and 10.4 s, and for some of these, 2_-^{SR}, 2_-^{MR}, and 2_+^{MR} whistlers are also recognizable. The multicomponent whistlers enhance the hiss band below ~1 kHz, consistent with previous research on lightning as an embryonic source of hiss (*12*). (**B**) Whistlers that have crossed the equator six times, 6_-^{SR}, 6_-^{MR}, 6_+^{SR}, and 6_+^{MR}, are better identified in this zoomed version of (A) between 6 and 9 s.

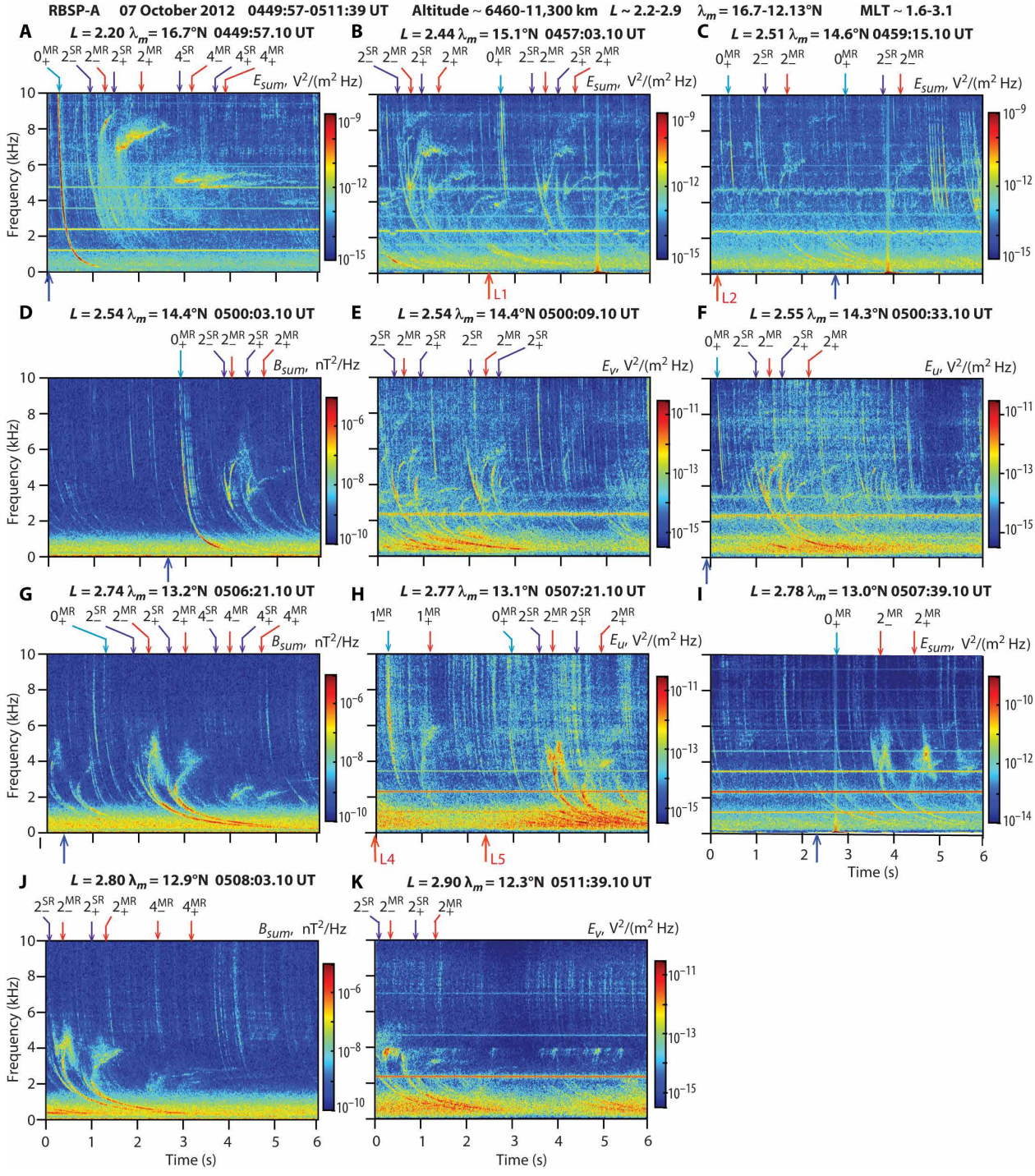

Fig. 3. Observations of a series of SR and MR whistlers on the RBSP-A. (**A** to **K**) SR and MR whistlers were observed in all 6-s frames of wideband wave data recorded on 07 October 2012 over an ~20-min orbit segment covering an ~0.7 L-shell range. Red arrows (labeled L1, L2, L4, and L5) show the times of the causative lightning flashes detected by the WWLLN that could be associated with multicomponent SR and MR whistlers that follow the lightning flashes within ~0.5 to 1 s. (G) The same whistlers as those in Fig. 1A. The time L3 of causative lightning flash associated with the first set of whistlers in (G) is not shown in the figure (see Fig. 1 caption). Blue arrows show the estimated times of causative lightning, not detected by the WWLLN, for the intense multicomponent whistlers. The estimated lightning flash times for weaker whistlers are not shown.

methods well established in the literature (text S2). Figure 4 and fig. S5 show the lightning flashes recorded by WWLLN during the interval when whistlers shown in Fig. 3 and fig. S4 were observed, respectively. Note that the WWLLN recorded 170 lightning flashes during the ~22-min interval shown in Fig. 4. During this period, RBSP-A recorded 11 6-s frames of broadband data (Fig. 3), for a total of 66 s, with each frame showing multiple whistlers originating in more than one flash. We surmise that most of the lightning flashes detected by the WWLLN produced detectable whistlers in the magnetosphere. On the other hand, our research indicates that, for many whistlers (e.g., whistlers following blue arrows in Fig. 3 and fig. S4), causative lightning flashes could not be found in the lightning data, consistent with the limited detection efficiency of the WWLLN (*37*). We note that, in all cases when a multicomponent SR-MR whistler could be unambiguously associated with lightning flash recorded by the WWLLN (indicated by red arrows in Fig. 3 and fig. S4), we found that the lightning flash occurred at low geomagnetic latitudes (<21°) (see tables S1 and S2). Table S1 shows that lightning flashes covering a wide range of energy, from ~250 to ~14,000 J, produced SR and MR whistlers. Table S2 shows that the lightning flash as far away as ~3000 to 4000 km from the ionospheric injection point could produce detectable SR and MR whistlers on a satellite located around L ~ 2.5 in the equatorial region. A whistler propagation model, discussed later in Materials and Methods, predicts that, in general, lightning flashes occurring at low geomagnetic latitudes ($\lesssim$30°) should produce SR and MR whistlers of comparable intensities, consistent with the observations reported above.

A survey of RBSP-A and RBSP-B wave data from the Oct 2012 to Nov 2012 period (text S4) (*38*) showed that both SR and MR whistlers are commonly observed inside the plasmasphere over the L-shell range of ~1.9 to 3.8, the latitude range of ~18°S to 17°N (limited by Van Allen Probes orbit inclination), and during geomagnetically quiet to moderately disturbed conditions. The maximum in the planetary Kp index 24 hours prior to the detection of whistlers ranged between 0.33 and 6. Both SR and MR whistlers are detected more frequently at nighttime than at daytime. At daytime, a greater number of MR whistlers are observed compared to the number of SR whistlers; at nighttime, both are observed with roughly equal frequency. When observed simultaneously, the intensity of both MR and SR whistlers is comparable during nighttime and daytime. In general, the occurrence patterns of SR and MR whistlers are consistent with the occurrence properties of lightning, including flash frequency and intensity (*39*–*42*), and the predictions of the whistler propagation model (see Materials and Methods, "Whistler propagation model" section) discussed below.

Quantitative confirmation of the SR whistler phenomenon

Ray tracing simulations quantitatively confirm the interpretation given above by reproducing the observed dispersion and cutoff frequencies of the whistlers shown in Fig. 1A (see Materials and Methods, "Ray tracing program" section).

Figure 5A shows the ray tracing simulation results in a smooth magnetosphere with a horizontally stratified ionosphere (tables S3 to S5, fig. S6A, and text S5). The simulation results (cyan, blue, and red curves) generally agree with the observations (gray curves) for set 2 SR and MR whistlers. Still, there are a few discrepancies in the upper cutoff frequencies and time delays. Commonly present field-aligned irregularities (FAIs) in the ionosphere can tilt the wave normal angle of injected waves by a few degrees, thus altering the ray paths reaching the satellite and affecting the time delay and cutoff frequencies (*43*, *44*). Figure 5B shows that the ray tracing calculations in a magnetosphere containing FAIs lead to a better agreement between simulation results and the observations (text S6). The ray tracing simulations also confirm that, (i) at all frequencies, rays injected at lower latitudes generate SR, and those at higher latitudes generate 0_+ MR and MR whistlers; (ii) the wave normal angles of

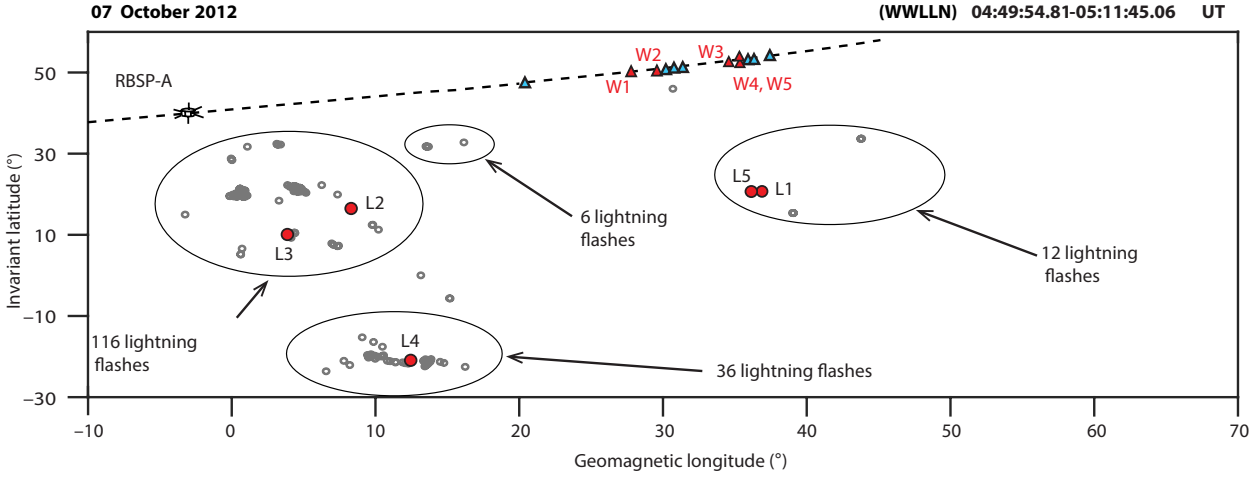

Fig. 4. Association of whistlers observed on the RBSP-A on 07 October 2012 with lightning activity recorded by the WWLLN. The black dashed curve shows the RBSP-A satellite footprint in the dipole coordinate system (Λ_m and ϕ_m), where Λ_m is the invariant latitude. The dashed curve shows the geomagnetic footprint of the satellite orbit. The cyan and red triangles give the locations of the footprint of the satellite when the 6-s frames of wideband whistler data were recorded (see Fig. 3). Gray open circles show the locations of lightning flashes recorded by the WWLLN during the ~20-min interval when whistlers were observed on the RBSP-A satellite. The red solid circles give the locations of the lightning flashes L1 to L5, recorded by the WWLLN, that are associated with whistlers seen in Fig. 3 (B, C, G, and H), and the red triangles W1 to W5 give the locations of the satellite orbit footprint when these whistlers were observed. The blue triangles give the locations of the whistlers associated with lightning flashes (not recorded by the WWLLN) indicated by blue arrows in Fig. 3. Note that each of the five lightning flashes (red solid circles) associated with SR and MR whistlers occurred at low geomagnetic latitudes (<21°; see also tables S1 and S2).

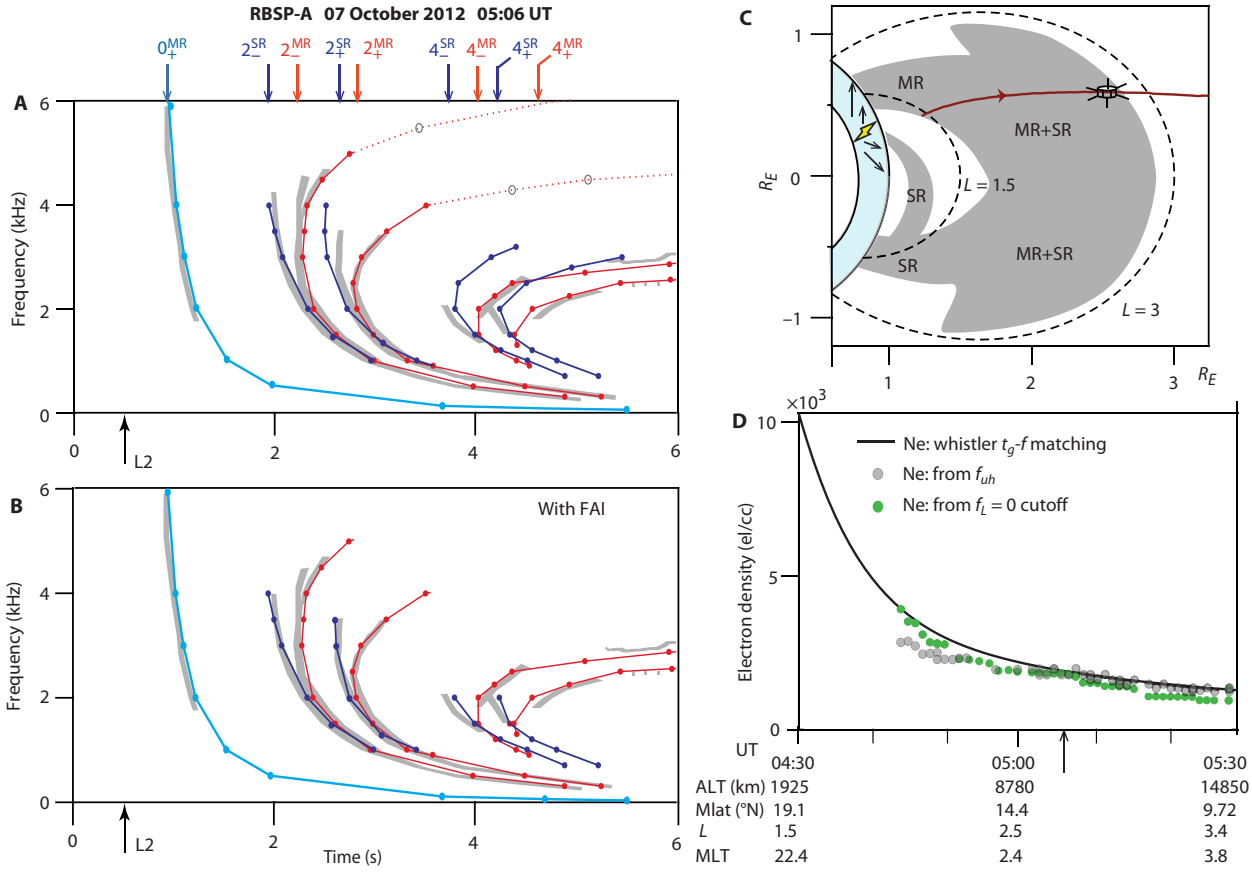

Fig. 5. Ray tracing simulations of lightning energy propagation to the RBSP-A satellite. (**A**) Comparison of the observed dispersion (gray curves) of the set 2 whistlers shown in Fig. 1A with that obtained from ray tracing simulations (cyan, blue, and red curves) in a smooth magnetosphere with a horizontally stratified ionosphere. (**B**) Same as (A) but assuming propagation to be in the magnetosphere used in the ray tracing simulation of (A) but with the ionosphere containing FAIs below ~500-km altitude. (**C**) In the magnetic meridional plane containing RBSP-A (ϕ_m = 34.5°E), the gray region (L ~ 1.1 to 2.85, λ_m ~ ±42°) shows the collection of the ray paths of 1- to 6-kHz signals that simulate the propagation of observed whistlers. The red curve shows the projection in the meridional plane of RBSP-A's orbit from 04:30 to 05:30 UT. The satellite location is shown at L = 2.75, where the whistlers shown in Fig. 1A were observed. Dipole field lines (dashed curves) at L = 1.5 and 3.0 are shown for reference. (**D**) Comparison of electron density along the satellite orbit measured by the HFR instrument on RBSP-A (green and black open circles) with that obtained from the ray tracing density model (black curve). The arrow on the time axis indicates the time of whistler observation.

corresponding MR and SR whistlers reaching the satellite are large and within a few degrees of each other (see columns 4 and 5 of table S5), consistent with the observed intensities of SR and MR whistlers on three magnetic antennas, as noted earlier. Further analysis of EMFISIS six-component wave data for the whistlers shown in Fig. 1 using recent methods (*45*) of wave normal angle and the Poynting vector direction is required to quantitatively verify wave normal angle and ray directions predicted by ray tracing simulations. However, such an analysis performed for another case (*28*) demonstrated an excellent agreement between the wave normal angle and Poynting vector direction predicted by ray tracing analysis and those measured from the six-component wave data (see text S7, figs. S6C, S7, and S8, and tables S3, S4, and S6).

Figure 5C shows the two-dimensional (2D) region (gray area) in the magnetic meridional plane covered by the ray paths of lightning energy in the 1- to 6-kHz range reaching the satellite. The time delay accrued by each ray reaching the satellite depends on the electron density and ion composition it encounters along its path, implying that the observed dispersion of SR and MR whistlers can provide electron and ion composition in the gray region. Figure 5D shows that the in situ electron density along the satellite path (red curve in Fig. 5C) obtained from the upper hybrid resonance band observed by the high-frequency receiver (HFR) instrument on the RBSP-A satellite (see Materials and Methods, "Instrumentation, datasets, and data analysis methods" section, fig. S9, and text S8) agrees well with that from the ray tracing density model. Excellent agreement between the observed and simulated whistlers and the ray tracing density model and measured electron density underscores the potential of a ray tracing inversion method (*46*) for obtaining the 2D images of the magnetospheric electron density and ion composition from whistler measurements (text S9) (*47*).

A recently developed whistler propagation model (see Materials and Methods, "Whistler propagation model" section, fig. S10, and table S7) provides further quantitative confirmation of the SR whistler phenomenon by reproducing relative intensities of the observed SR and MR whistlers. The whistler propagation model takes into account source lightning intensity and various propagation losses, including those in the E-I waveguide (*48*), transionospheric propagation

(*49*), and defocusing in the magnetosphere (*23*). We apply this model to whistlers observed on 07 October 2012 (Fig. 1) to demonstrate that it explains the observed relative intensities of 2_- and 2_+ SR and MR whistlers (text S10 and tables S8 and S9).

The SR and MR intensity measurements coupled with the whistler propagation model and ray tracing simulations lead to powerful methods of ionospheric diagnostics, including the determination of poorly known E-I waveguide (*4*, *48*, *50*) and transionospheric losses (*4*, *49*), and the altitude of specular reflection (*46*, *51*). Whistler intensity measurements also allow remote sensing of a lightning flash intensity and location (text S11).

Figure 6 shows the spectral forms (t_g-f) of the simulated SR and MR whistlers in a typical magnetosphere (tables S3 and S4, fig. S6B, and text S12). The spectral forms depend on the latitude of the satellite location and whether or not the lightning is located in the same hemisphere as the satellite. When the satellite is at low latitudes, the same order SR and MR before reflection in the hemisphere of satellite (e.g., 2_-^{SR} and 2_-^{MR}) and after reflection in the hemisphere of satellite (e.g., 2_+^{SR} and 2_+^{MR}) that occur in pair with their spectra appear to be merging at low frequencies, as seen in Fig. 6 (B and C). Van Allen Probes with low inclination orbit observe SR and MR whistlers with spectra similar to those in Fig. 6 (B and C). When the satellite is at high latitudes in the region close to altitudes where magnetospheric reflections occur, the SR whistlers of the same order (e.g., 2_-^{SR} and 2_+^{SR}) and MR whistlers of the same order (e.g., 2_-^{MR} and 2_+^{MR}) have their spectra that appear to merge near their lower cutoff frequencies, similar to those seen in Fig. 6 (D and E). Such whistlers were observed on high-inclination Orbiting Geophysical Observatory 1 (OGO 1) satellite (*5*, *21*, *52*). While the characteristics of SR and MR whistlers are different for low- and high-latitude observations, in all cases, the SR and MR whistlers have spectra similar enough that an SR whistler could be easily mistaken for an MR whistler and vice versa. This may explain why SR whistlers were not found earlier. Early researchers who observed spectral forms similar to SR whistlers interpreted them, we believe mistakenly, as MR whistlers resulting due to refraction from large-scale magnetospheric density depressions (*5*, *21*). The SR whistler phenomenon we report here is lightning energy injected at lower latitudes in a smooth magnetosphere. It is distinct from and coexists with the MR whistler phenomenon, which originates in lightning energy injected at higher latitudes.

Lightning energy reaching the magnetosphere as SP, SR, MR, and ducted whistlers

Previous ray tracing studies concluded that, while the lightning energy injected at higher latitudes (>20° to 30°) reached the magnetosphere as MR whistlers, the lightning energy injected at lower latitudes was unable to escape the ionosphere (*18*, *29*). Contrary to this result, we have shown above that the lightning energy injected at low latitudes can reach the magnetosphere as SR whistlers. This

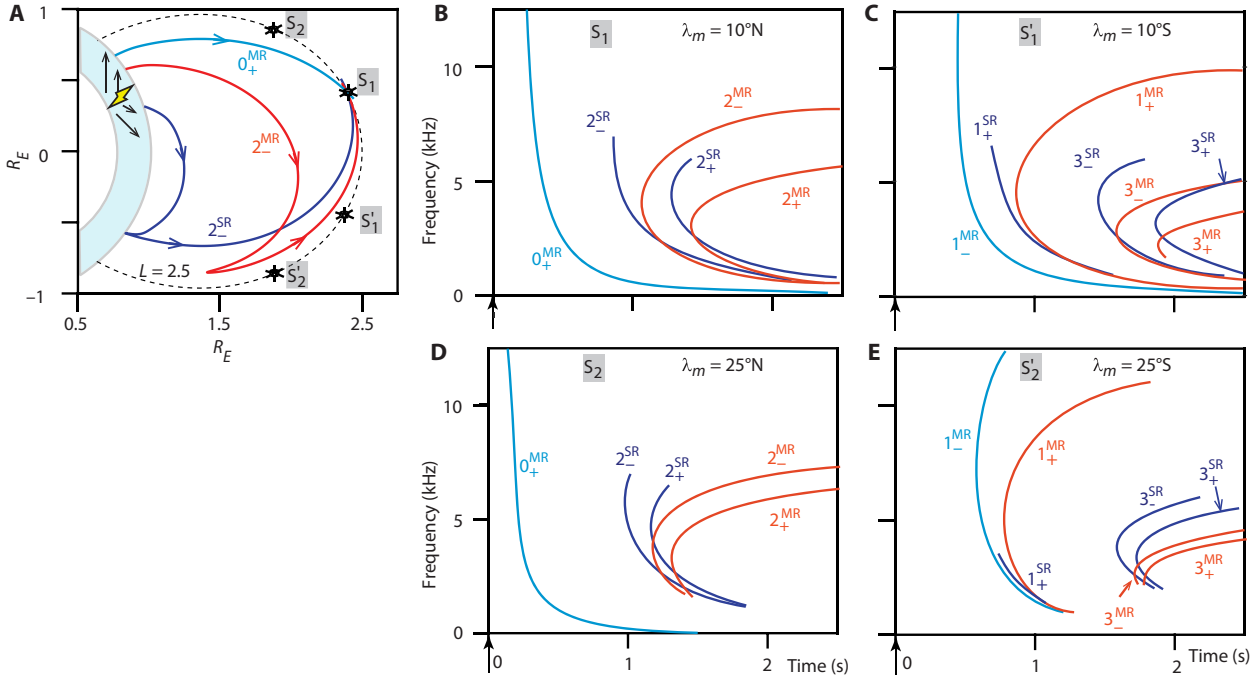

Fig. 6. Expected spectral forms of SR and MR whistlers in a typical magnetosphere when the lightning flash location is in the Northern Hemisphere. (**A**) Ray paths of 3-kHz waves injected from the lightning (yellow symbol) and reaching the satellite located at S_1 ($L = 2.5$, $\lambda_m = 10°$N) via a direct path (0_+; cyan), after a magnetospheric reflection (2_-^{MR}; red), and after a specular reflection (2_-^{SR}; blue). The black dashed curve represents the $L = 2.5$ field line. (**B**) Expected spectral forms of SR and MR whistlers when the satellite is located at S_1($L = 2.5$, $\lambda_m = 10°$N) in the hemisphere of the causative lightning. (**C**) Same as (B) when the satellite is at S_1' ($L = 2.5$, $\lambda_m = 10°$S) in the hemisphere conjugate to that of the causative lightning. SR and MR whistlers with dispersion similar to that of simulated whistlers shown in (B) and (C) are observed on Van Allen Probes. (**D**) Same as (B) when the satellite is at S_2 ($L = 2.5$, $\lambda_m = 25°$N), a high-latitude location in the hemisphere of the causative lightning. (**E**) Same as (B) when the satellite is at S_2' ($L = 2.5$, $\lambda_m = 25°$S), a high-latitude location in the hemisphere conjugate to that of the causative lightning. SR and MR whistlers with dispersion similar to those of simulated whistlers shown in (B), (C), and (D) were observed on high-inclination OGO 1 satellite (*5*, *21*, *52*).

discovery may have profound significance for radiation belt physics, as discussed below. Our research shows that (i) the lightning energy couples to the magnetosphere primarily as nonducted SR and MR whistlers, a small fraction as ducted whistlers and another small fraction as SP whistlers (altitude $\lesssim$ 1000 km), and (ii) the energy contributions of SR and MR whistlers are comparable. We performed ray tracing studies in a typical magnetosphere to determine (i) the injection latitude ranges for lightning energy that leads to the generation of SR, MR, and SP whistlers; (ii) ionospheric and magnetospheric regions where these whistlers are found; and (iii) the relative amounts of lightning energy reaching the magnetosphere as SR, MR, SP, and ducted whistlers.

As discussed above, the lightning energy enters the ionosphere almost vertically. We injected rays vertically at the E-I boundary in the 1- to 11-kHz frequency range, roughly the range in which SR and MR whistlers are typically observed (Figs. 1 to 3, and figs. S4 and S7) (*5*), and between ~0° and 60° geomagnetic latitudes. In a typical magnetosphere with plasmapause near $L = 4$, the lightning energy injected at latitudes near 60° gets trapped in the plasmapause, which acts as a waveguide (*53*). We allowed rays to propagate until $t_g = 20$ s, roughly the time in which whistlers are observed to merge with the background radiation (*12*).

Figure 7A shows the lightning energy injection latitude ranges for 1- to 11-kHz frequency range for each type of whistler (text S13 and figs. S11 and S12). While the key feature of this figure, that SP and SR whistlers are generated with lower injection latitudes for lightning energy and MR whistlers with higher, holds in general, the numerical values of the latitude ranges for each kind of whistler will depend on the magnetospheric density model used. Ionospheric latitudinal gradients and FAIs influence the ray paths and thus modify the injection latitude ranges and the subsequent propagation of the whistlers (fig. S13 and text S14). As the magnetospheric plasma density and composition change diurnally or with geomagnetic activity, we expect that these injection latitude ranges to change accordingly.

Figure 7 (B to D) shows, as a function of frequency, the equatorial L-shell ranges reached by direct ($0_+/1_-$) SR and MR whistlers, higher-order (1_+, 2_-, 2_+, …) SR, and higher-order (1_+, 2_-, 2_+, …) MR whistlers, respectively. The hatched regions ($1.5 \lesssim L \lesssim 3.2$) in Fig. 7 (B and C) show roughly the equatorial L-shell ranges where the lightning energy injected at various latitudes reaches as SR and MR whistlers in 20 s. In the L-shell ranges covered by the hatched region, we expect to find a buildup of whistler energy that, via wave-particle interactions, may contribute to the formation of the radiation belt slot region (*18*, *54*). The lower boundary of the hatched region approaches equatorial lower hybrid frequency ($f_{lh,eq}$) for both SR and MR whistlers, noted previously for MR whistlers (*54*). Ray tracing (Figs. 1, B and C, and 5C, and fig. S11C) shows that we expect to observe SR and MR whistlers within roughly ±40° geomagnetic latitudes, determined by the latitudes of magnetospheric reflections. The equatorial L-shell ranges of SR and MR whistlers shown in Fig. 7 (B to D) are consistent with those found for these whistlers in the Van Allen Probes data survey discussed above (see text S4).

Energy from an individual lighting flash propagates in all directions in the E-I waveguide and is injected into the ionosphere at the E-I waveguide boundary at all latitudes and longitudes. The relative amounts of lightning energy reaching the magnetosphere as nonducted SR, MR, and SP and ducted whistlers are calculated using (i) the whistler propagation model (see Materials and Methods, "Whistler propagation model" section) that takes into account the injection latitude ranges for these whistlers (Fig. 7A) and the E-I waveguide (*48*) and transionospheric (*49*) losses; (ii) the global lightning occurrence as a function of latitude (fig. S14) (*39*, *40*); (iii) duct occurrence probability (*8*); and (iv) effective duct area at the E-I boundary (*20*, *55*).

Figure 8 (text S15) shows, as a function of geomagnetic latitude of lightning flash, the relative contribution of lightning energy to the magnetosphere as SR, MR, and SP whistlers in 1- to 11-kHz frequency band due to a single lightning flash (Fig. 8A) and due to global lightning flashes per second (Fig. 8B). Figure 8 (A and B) shows that a lightning flash contributes greater energy to the magnetosphere at nighttime relative to daytime and comparable energy as SR and MR whistlers when a lightning flash occurs at low geomagnetic latitudes, $|\lambda_m^L| \lesssim 25°$ to 30°, where $|\lambda_m^L|$ is the lightning flash geomagnetic latitude. These results are consistent with our observations that SR and MR whistlers are detected simultaneously, with comparable intensity, and more frequently when the lightning flash is at low geomagnetic latitudes ($|\lambda_m^L| \lesssim 30°$) and at nighttime (Figs. 1 to 4, figs. S4 and S5, and table S2).

Integrating relative energy contributions to the magnetosphere of SR, MR, and SP whistlers shown in Fig. 8B over $-90° \leq \lambda_m^L \leq 90°$ and 24-hour period, we get the following results for global lightning

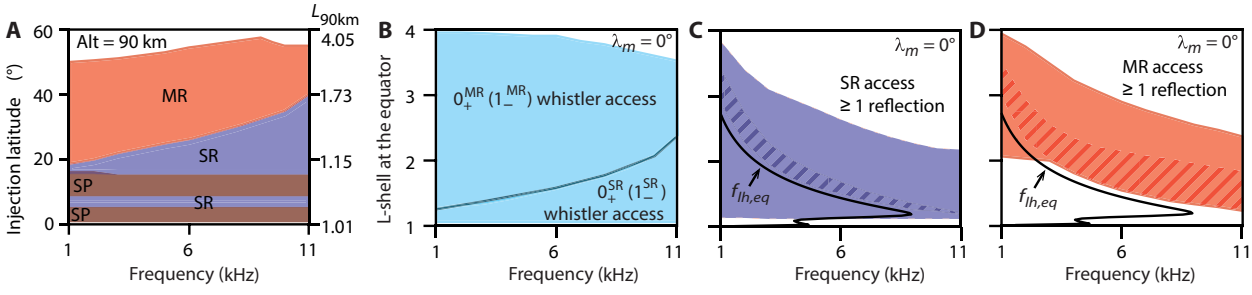

Fig. 7. Lightning energy injection latitude ranges for SP, SR, and MR whistlers and equatorial accessibility of SR and MR whistlers. (**A**) Lightning energy injection latitudes at the E-I boundary and the corresponding L-shell (right *y* axis) leading to the generation of SP, SR, and MR whistlers. (**B**) The cyan-colored region represents the L-shell ranges at the equator as a function of frequency reached by 0_+^{MR} and 1_-^{MR} whistlers (above the blue solid line) and 0_+^{SR} and 1_-^{SR} whistlers (below the blue solid line). The SP whistlers (not shown in the figure) are observed below 1000 km. (**C**) The blue area represents the equatorial L-shell range as a function of frequency reached by SR whistlers after one or more reflections. The hatched dark blue region represents the L-shell range as a function of frequency at the equator reached by SR whistlers after propagating for 20 s. The black solid curve is the equatorial lower hybrid frequency as a function of L-shell. (**D**) Same as (C) but for MR whistlers.

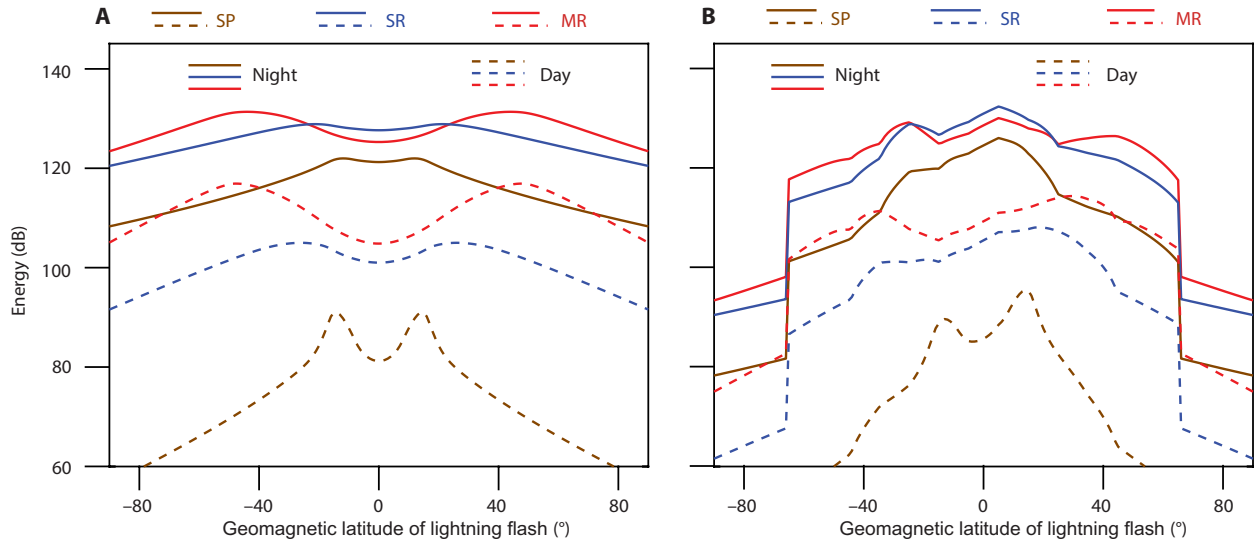

Fig. 8. Relative contributions of SP, SR, and MR whistlers to the lightning energy reaching the magnetosphere. (**A**) Relative contributions of SP, SR, and MR whistlers to the lightning energy reaching the magnetosphere as a function of the geomagnetic latitude of a lightning flash. (**B**) Relative contributions of SP, SR, and MR whistlers to the lightning energy reaching the magnetosphere per second as a function of the geomagnetic latitude from global thunderstorm activity. This calculation takes into account the lightning flash frequency as a function of latitude (fig. S14) (*39*, *40*).

energy reaching the magnetosphere per day: (i) The lightning energy reaching the magnetosphere at nighttime is ~20 dB greater than that reaching at daytime; (ii) SR and MR whistlers carry equal (within 1 dB) amounts of lightning energy to the magnetosphere; (iii) SP whistlers, i.e., the lightning energy trapped in the ionosphere ($\lesssim$1000 km), carry energy that is about 10 dB lower than that reaching the magnetosphere as SR and MR whistlers; and (iv) ducted whistlers carry about 1 to 4% of the lightning energy entering the ionosphere, about 14 to 20 dB lower than the total nonducted whistler energy reaching the magnetosphere (table S10 and text S16). We can understand the roughly equal contribution of SR and MR whistlers to lightning energy reaching the magnetosphere by recognizing that (i) most lightning activity takes place at low latitudes that are close to SR injection latitudes, and thus, the E-I losses are lower for SR whistlers compared to MR whistlers, and (ii) transionospheric losses, which are greater at low latitudes, are higher for SR whistlers compared to MR whistlers. If we consider that the lightning flashes at lower latitudes are more intense than those at higher latitudes (*41*, *42*), then SR whistlers probably carry a greater part of lightning energy to the magnetosphere relative to that carried by MR whistlers.

DISCUSSION

Storey demonstrated in his 1953 breakthrough paper that lightning is the source of terrestrial whistlers (*1*). Since then, whistlers, their interactions with radiation belt particles, and their applications for magnetospheric diagnostics have been the subject of vigorous research. Various types of whistlers, including ducted, nonducted, SP, and MR whistlers, were found in the 1950s and 1960s (*1*–*5*). Here, we report the discovery of SR whistler, which carries the lightning energy injected at low latitudes to the magnetosphere. Because most lightning activity occurs at low latitudes, the contribution of SR whistlers to the magnetosphere is comparable to that of MR whistlers despite greater transionospheric losses at lower latitudes. Comparatively, a small fraction of lightning energy injected at low latitudes remains trapped in the ionosphere as SP whistlers. The importance of our research lies not only in the discovery and interpretation of the SR whistlers but also in demonstrating the significance of these whistlers in their impacts on the radiation belt particles and their implications for new magnetospheric and ionospheric diagnostics.

One may ask why the SR phenomenon was not identified before. As noted above, previous researchers observed whistlers with spectra similar to those shown in Fig. 1A on OGO 1 satellites (*5*, *21*); however, they interpreted those spectra as additional MR whistler traces resulting from multipath propagation of lightning energy injected at higher latitudes and refracted by large-scale density depressions in the magnetosphere. In our interpretation, SR and MR whistlers are generated in a smooth magnetosphere with lightning energy injected at lower latitudes reaching the satellite as SR and at higher latitudes as MR. Thus, our interpretation does not require the presence of large-scale irregularities in the magnetosphere; furthermore, our interpretation shows that the lightning energy reaching the magnetosphere is doubled when we consider SR whistlers. Because the spectra of SR and MR whistlers are similar (Fig. 6), the earlier authors, we speculate, probably interpreted SR whistlers as MR whistlers.

Independent of observations, ray tracing simulations predict SR and MR whistlers. Our ray tracing calculations shown above predict the generation of SR and MR whistlers and provide quantitative confirmation of the observed dispersion of these whistlers (Fig. 5). Similar to our ray tracing simulations, some of the past works on ray tracing simulations (*18*, *29*, *56*) showed that rays injected at low latitudes propagate to conjugate hemisphere ionosphere, but unlike our ray tracing simulations, these authors did not consider specular reflection in the conjugate hemisphere that is required for lightning energy to propagate to the magnetosphere.

It may interest the reader that the search for SR whistlers was inspired by the authors' work on whistler mode radio sounding

from the Imager for Magnetopause-to-Aurora Global Exploration (IMAGE) satellite (*46*, *57*). This work showed that whistler mode signals at very low frequencies injected from the IMAGE satellite resulted in unexpectedly strong obliquely incident SR echoes that implied an efficient specular reflection of whistler energy, notwithstanding previous works that implied large D-region absorption at low latitudes (*4*, *23*, *58*).

Role of caustics

Previous research has shown that the magnetospheric region where MR whistlers are observed is bounded by frequency-dependent exterior and interior caustics (*34*, *55*, *56*). The interior caustic forms the boundary between $0_+/1_-$ MR and $0_+/1_-$ SR whistlers. Our ray tracing results (see Fig. 7A) indicate the existence of additional caustics that form boundaries between magnetospheric regions where SR, SR-SP, and SP whistlers are expected to be observed. Further research involving conjunction experiments between low- and high-altitude satellites is required to study these caustics and the injection latitude ranges of SR, MR, and SP whistlers shown in Fig. 7A.

Role of FAIs and ground penetration of SR whistlers

The influence of ionospheric FAIs of ~1- to 10-km scale and latitudinal gradients on the propagation of whistler mode waves injected from the ground is well established in the literature (*43*, *44*). Ray tracing analysis of the 07 October 2012 case has shown that ionospheric FAIs can modify both the cutoff frequencies and dispersion of whistlers. FAIs can also modify the injection latitude ranges for lightning energy that lead to SR, MR, and SP whistlers (see fig. S13), and hence, the magnetospheric regions where these whistlers can be observed. Ray tracing analysis of whistler striations observed on OGO 4 has shown that equatorial anomaly, commonly present in the evening time low-latitude ionosphere, can modify the ray propagation paths of whistler mode signals injected from the ground (*56*). Therefore, we speculate that equatorial anomaly may modify the SR whistler propagation paths and spectra. Past research on the ground observations of auroral hiss and chorus (*59*, *60*) indicates that, in the presence of small-scale ionospheric FAIs (~1 to 10 m), whistler mode waves approaching the E-I boundary at large wave normal angles may be observed on the ground. This result implies that 1_-^{SR} whistlers may be detected on the ground in the presence of small-scale FAIs. Ground-satellite conjunction experiments should be able to test the transmission of SR whistlers to the ground. It is possible that some of the whistlers observed in the past at low-latitude ground stations (*61*) may be SR whistlers. A comparison of the dispersion of low-latitude whistlers with that expected from ray tracing simulations may be another way to test the SR whistler transmission to the ground.

Altitude of specular reflection

Specular reflection of whistler mode waves approaching the E-I boundary from above is a little researched topic. The propagation theory predicts two possible locations for specular reflections: (i) near the F2 peak (*51*), in which case the wave would not suffer attenuation, and (ii) near the E-I boundary, where the wave would suffer large attenuation due to D-region absorption (*4*). As discussed above, the application of the whistler propagation model to the 07 October 2012 case supports reflection near the F2 peak. Analyzing SR whistlers allows one to study the altitude of specular reflection and its variation with day/night and geomagnetic activity. Past research on explaining quasi-periodic emissions using ray tracing simulations has shown that ray tracing simulations can distinguish between a reflection just below the F2 peak and one at the E-I boundary (*51*). Therefore, we believe that comparing dispersion predicted by ray tracing simulations with that obtained from whistler measurements can provide the reflection altitude, and the comparison of the ratio of SR and MR whistler intensities predicted by the propagation model with the measured one should provide wave attenuation in specular reflection.

Magnetospheric and ionospheric diagnostics

Whistler dispersion has been effectively used for magnetospheric diagnostics of equatorial electron density as a function of L-shell (*4*, *5*, *62*). Our research has shown that this method can be extended to 2D imaging of the magnetospheric electrons and ions (text S9) (*47*). The success of the propagation model in explaining the relative intensities and the occurrence patterns of SR and MR whistlers suggests that the intensity of whistlers is another observable parameter that can provide new diagnostics of E-I waveguide losses, transionospheric losses, defocusing losses, losses in specular reflection, and determination of lightning flash location and intensity (text S11) (*23*, *48*, *49*).

Impact of SR whistlers on radiation belts

Because SR and MR whistlers carry roughly equal amounts of lightning energy to the magnetosphere, occupy similar regions of the magnetosphere with similar wave normal angles and intensities, and, in time, settle down at similar L-shells, we expect that SR whistler interactions with radiation belt particles should be similar and comparable to that of MR whistlers for the precipitation of energetic particles (*6*–*11*), the generation of hiss (*12*–*16*), and the formation and sustenance of slot region (*10*, *11*, *17*, *18*, *54*). Therefore, we believe that previous calculations of lightning impact on radiation belts that took only MR and ducted whistlers into account need to be substantially revised. Further research should be done on the detailed calculations of the impact of SR whistlers on radiation belts using methods developed by previous researchers for MR whistlers (*9*, *10*, *13*, *18*, *54*).

Limitations of this study

While plasma wave data from Van Allen Probes have provided a large number of SR whistlers for our study, one limitation of our dataset is that, because of their low orbital inclination, Van Allen Probes provide data on whistlers observed near the equatorial magnetosphere with spectra similar to those shown in Fig. 6 (B and C). Data from high-inclination or polar-orbiting satellites, such as POLAR and CLUSTER, which cover low and high geomagnetic latitudes, should provide MR and SR whistler observations with spectra similar to those shown in Fig. 6 (B to E). Some studies require whistler measurements at high latitudes, which are unavailable on Van Allen Probes. For example, the lower cutoff frequencies of MR and SR whistlers observed at high latitudes provide values of f_{lh} (and thus ion composition) at the satellite location (*52*). Our interpretation predicts that lightning flash occurring close to the geomagnetic equator should provide two sets of SR and two sets of MR whistlers, one resulting from the lightning energy injected from the Northern Hemisphere and the other from the Southern Hemisphere. The spectra of these two sets would nearly overlap for observations made close to the equator but would be well separated for observations

made at higher latitudes. Furthermore, the direction of propagation determined by the Poynting vector of two sets of whistlers would be opposite. Plasma wave data from high-inclination orbit satellites should contain examples of such whistlers.

We conclude that SR whistler is a common magnetospheric phenomenon that carries a substantial portion of the lightning energy reaching the magnetosphere and arguably plays an important role in the physics of the radiation belts. The dispersion of SR and MR whistlers coupled with ray tracing simulations provide a method for obtaining 2D images of magnetospheric plasma density and composition. The intensities of SR and MR whistlers coupled with the whistler propagation model provide new methods of measuring E-I waveguide and transionospheric losses and remote sensing of lightning flash location and intensity.

MATERIALS AND METHODS

Instrumentation, datasets, and data analysis methods

Van Allen Probes

The twin Van Allen Probe spacecraft (RBSP-A and RBSP-B), launched in August 2012, carried identical scientific payloads and flew in nearly identical orbits with a perigee altitude of 500 to 675 km, an apogee altitude of ~30,050 to 31,250 km, and an inclination of ~10° (*30*). The spacecraft orbit covers ~1.1 to 6.0 L-shell range and ~20°N to 20°S geomagnetic latitude range. As each probe ran out of fuel, Van Allen Probe B was deactivated on 19 July 2019, and Van Allen Probe A was deactivated on 19 October 2019, bringing the mission to a close. The fundamental purpose of the mission is to provide a better understanding of the processes that drive changes within the Earth's radiation belts. Van Allen Probes's orbit characteristics permit observations of whistler mode waves, including lightning-generated whistlers and their interactions with the radiation belt particles near the equatorial plane in the inner magnetosphere (https://space.jhuapl.edu/destinations/missions/van-allen-probes).

EMFSIS instrument suite

The EMFISIS suite includes a WFR that measures three magnetic (B_u, B_v, and B_w) and three electric (E_u, E_v, and E_w) components of plasma waves in the frequency range of 10 Hz to 12 kHz using triaxial search coils and the triaxial electric field sensors (*31*, *63*). The EMFISIS suite also has an HFR that measures a single electric field component of waves in the frequency range of 10 to 500 kHz. The search coils consist of 40-cm mu-metal cores wound with 10,000 turns of fine copper wire. The electric field signals are obtained from the triaxial electric field booms of the electric fields and waves instrument that has a cutoff frequency of 400 kHz (*64*). The electric field booms are parallel to the three search coil axes with two of the booms in the spacecraft spin plane having lengths of 100 m tip to tip and the axial boom perpendicular to the spin plane having a tip-to-tip length of ~14 m. The WFR simultaneously samples all six channels with a 35-kHz sampling rate and 16 bits of digitization. The HFR has a selectable input but is usually connected to one of the spin plane booms and samples the electric field at a rate of 1.25 million samples per second with 14-bit digitization. EMFISIS also includes a fluxgate magnetometer, which provides measurements of |B|, used here to determine electron cyclotron frequency, f_{ce}.

Use of WFR data for whistler observations and analysis

The orbit of Van Allen Probes is well suited to study the equatorial processes in the inner magnetosphere, particularly those related to radiation belts. Over the 7-year lifetime of Van Allen Probes, the EMFISIS instrument suite regularly observed naturally occurring plasma waves, including whistlers, hiss, chorus, and upper hybrid emissions, among others (*31*, *63*, *65*, *66*).

Whistler observations reported here were made using the 6-s burst data obtained by the WFR. The spectrogram of one of the electric or magnetic field components was used to scale the data for dispersion curves (t_g-f) by visual inspection and using a web-based digitizer to scale the t_g-f data from the spectrogram of (https://apps.automeris.io/wpd/).

The combined power spectra of three electric and magnetic field components were used to measure whistler electric and magnetic field intensities. The product of electric field and magnetic field intensities was used to estimate the power spectral density carried by the wave. This method of estimating power spectral density is adequate for calculations carried out here, namely, the ratio of the lightning energy carried by SR and MR whistlers to the magnetosphere. [MATLAB command spectrogram (x, 1024, 1000, 1024, 35×10^3, and "y axis") was used to find the power spectral density of each component of the electric and magnetic field, where x is the field component used to obtain the spectra for each component.]

Use of HFR data to determine in situ electron density

The upper cutoff frequency (f_{uh}) and the lower cutoff frequency ($f_{L=0}$) of the z-mode emission band measured by the HFR are used to determine in situ electron density (text S17) (*63*).

Association of lightning flashes and generated whistlers

WWLLN is a global very-low-frequency lightning location system using the time-of-group-arrival technique (*67*). It can detect cloud-to-ground (CG) and intracloud lightning, but the type of lightning is not distinguished in the data. This network improves in accuracy and detection efficiency with an increased number of stations. The number of lightning strokes located increased from 10.6 million to 28.1 million when the number of WWLLN stations increased from 11 in 2003 to 30 in 2007 (*68*). As of 2011, the network had an estimated detection efficiency of about 11% for CG lightning over the continental United States, and the number can increase to >30% for higher peak current lightning (*37*). At present, the WWLLN includes over 70 participating stations (https://wwlln.net).

The WWLLN provides positions, times, and several additional parameters of individual lightning strokes worldwide. Knowledge of individual stroke locations, with high temporal and spatial accuracy, is helpful for studying and relating whistlers observed on Van Allen Probes to their causative lightning. Because of the somewhat low detection efficiency of WWLLN, it is expected that we may not be able to find the causative lightning for every whistler detected on the satellite. On the other hand, weak lightning may not produce a detectable whistler on the satellite. However, in almost all cases of whistler observations on Van Allen Probes, we could identify the general locations of active thunderstorms that presumably contained the causative lightning flashes.

WWLLN archival data are copyrighted by the University of Washington and are available at a nominal cost (https://wwlln.net). The WWLLN data provide for each lightning flash the following parameters: Date and time are in universal time (UT); Lat, long in fractional degrees; Resid is the residual fit error in microseconds (always <30 μs); Nsta is the number of WWLLN stations that detected the stroke (always ≥ 5); energy (J), root mean square energy from 7 to 18 kHz in 1.3-ms sample time; energy uncertainty (J); and nstn_energy, a subset of Nsta within the range of 1000 to 8000 km distant from stroke and used for power estimate.

Several methods are used to associate lightning (thunderstorm) activity recorded by the WWLLN and the whistler observed on Van Allen Probes (text S2).

Ray tracing program

The Stanford 2D ray tracing program simulates whistler mode wave propagation in the magnetosphere (*46*, *53*). The program solves the Haselgrove equations (*69*) to determine the ray path in the magnetic meridional plane, assuming the magnetospheric density model described below.

The ray tracing program can successfully model magnetospheric reflection, which is a refraction that reverses the ray direction at altitudes where the wave frequency is approximately equal to the local lower hybrid resonance frequency f_{lh}. Ray tracing program cannot model the reflection near the E-I boundary where the refractive index undergoes a rapid change over a distance shorter than a wavelength, and the ray approximation (WKB) fails. The reflection at the E-I boundary is modeled as specular reflections (taking anisotropy into account) (*4*, *46*). Another possibility is that the specular reflection occurs close to the F2 peak altitude, typically ~250 km, where also the refractive index undergoes rapid change over a short distance (*51*). The specular reflection approach falls short of providing the type of full wave treatment that would be essential for a complete analysis. However, the past research using ray tracing simulations on modeling SR whistler mode echoes observed on IMAGE and modeling of propagation of quasi-periodic emissions observed on DEMETER show that the specular reflection assumption provides a close agreement between observations and simulations (*46*, *51*). Here, for all ray tracing simulations, we have assumed the specular reflection to take place at the E-I boundary. When calculating intensities of whistlers using the whistler propagation model (discussed below), we have considered both possibilities: (i) specular reflection at the E-I boundary, which would involve D-region absorption losses, and (ii) specular reflection just below the F2 peak, which would involve no absorption losses.

The Stanford ray tracing program (ray tracer) uses a dipole field model, a diffusive equilibrium model for density along field lines within the plasmasphere, and an (r^{-n}) density falloff outside the plasmasphere, where r is the geocentric distance (*46*, *53*). The plasma density model comprises several multiplicative modules, including a diffusive equilibrium module, a lower ionosphere module, a plasmapause module, and a duct module (text S18). The dipole field model is characterized by a single assignable parameter, $f_{ce,Eq}$, the gyrofrequency at the geomagnetic equator at the Earth's surface (*4*). For propagation at relatively low L-shells ($L \lesssim 4$) considered here, the dipole field model is a fair representation of the geomagnetic field. For analysis of whistlers observed at higher L-shell ($L \gtrsim 4$), a more accurate model, such as an International Geomagnetic Reference Field, may be needed.

Whistler propagation model

We have developed a whistler propagation model to predict the relative intensities of SR and MR whistlers and to determine the relative contributions of SR, MR, and SP whistlers to the lightning flash energy reaching the magnetosphere. The model takes into account various propagation losses, including E-I waveguide loss, transionospheric loss, and defocusing loss incurred by the lightning energy as it propagates from its source location to its reception point in the magnetosphere (text S19).

Supplementary Materials

This PDF file includes:

Supplementary Texts S1 to S19
Figs. S1 to S14
Tables S1 to S10
References

REFERENCES AND NOTES

1. L. R. O. Storey, An investigation of whistling atmospherics. *Phil. Trans. A Math Phys. Eng. Sci.* **246**, 113–141 (1953).
2. R. A. Helliwell, J. H. Crary, J. H. Pope, R. L. Smith, The "nose" whistler—A new high-latitude phenomenon. *J. Geophys. Res.* **61**, 139–142 (1956).
3. D. L. Carpenter, N. Dunckel, J. F. Walkup, A new very low frequency phenomenon: Whistlers trapped below the protonosphere. *J. Geophys. Res.* **69**, 5009–5017 (1964).
4. R. A. Helliwell, *Whistlers and Related Ionospheric Phenomena* (Stanford Univ. Press, 1965).
5. R. L. Smith, J. J. Angerami, Magnetospheric properties deduced from OGO 1 observations of ducted and nonducted whistlers. *J. Geophys. Res.* **73**, 1–20 (1968).
6. R. A. Helliwell, J. P. Katsufrakis, M. L. Trimpi, Whistler-induced amplitude perturbation in VLF propagation. *J. Geophys. Res.* **78**, 4679–4688 (1973).
7. H. D. Voss, W. L. Imhof, M. Walt, J. Mobilia, E. E. Gaines, J. B. Reagan, U. S. Inan, R. A. Helliwell, D. L. Carpenter, J. P. Katsufrakis, H. C. Chang, Lightning-induced electron precipitation. *Nature* **312**, 740–742 (1984).
8. W. C. Burgess, U. S. Inan, The role of ducted whistlers in the precipitation loss and equilibrium flux of radiation belt electrons. *J. Geophys. Res.* **98**, 15643–15665 (1993).
9. B. Abel, R. M. Thorne, Electron scattering loss in Earth's inner magnetosphere: 2. Sensitivity to model parameters. *J. Geophys. Res.* **103**, 2397–2407 (1998).
10. D. S. Lauben, U. S. Inan, T. F. Bell, Precipitation of radiation belt electrons induced by obliquely propagating lightning-generated whistlers. *J. Geophys. Res.* **106**, 29745–29770 (2001).
11. A. Green, W. Li, Q. Ma, X.-C. Shen, J. Bortnik, G. B. Hospodarsky, Properties of lightning generated whistlers based on Van Allen Probes observations and their global effects on radiation belt electron loss. *Geophys. Res. Lett.* **47**, e2020GL089584 (2020).
12. V. S. Sonwalkar, U. S. Inan, Lightning as an embryonic source of VLF hiss. *J. Geophys. Res.* **94**, 6986–6994 (1989).
13. A. B. Draganov, U. S. Inan, V. S. Sonwalkar, T. F. Bell, Magnetospherically reflected whistlers as a source of plasmaspheric hiss. *Geophys. Res. Lett.* **19**, 233–236 (1992).
14. J. L. Green, S. Boardsen, L. Garcia, W. W. L. Taylor, S. F. Fung, B. W. Reinisch, On the origin of whistler mode radiation in the plasmasphere. *J. Geophys. Res.* **110**, A03201 (2005).
15. O. Santolík, J. Chum, The origin of plasmaspheric hiss. *Science* **324**, 729–730 (2009).
16. O. Santolík, I. Kolmašová, J. S. Pickett, D. A. Gurnett, Multi-point observation of hiss emerging from lightning whistlers. *J. Geophys. Res.* **126**, e2021JA029524 (2021).
17. L. R. Lyons, R. M. Thorne, Equilibrium structure of radiation belt electrons. *J. Geophys. Res.* **78**, 2142–2149 (1973).
18. J. Bortnik, U. S. Inan, T. F. Bell, Energy distribution and lifetime of magnetospherically reflecting whistlers in the plasmasphere. *J. Geophys. Res.* **108**, 1199 (2003).
19. D. L. Carpenter, Whistler evidence of a 'knee' in the magnetospheric ionization density profile. *J. Geophys. Res.* **68**, 1675–1682 (1963).
20. J. J. Angerami, Whistler duct properties deduced from VLF observations made with the OGO 3 satellite near the magnetic equator. *J. Geophys. Res.* **75**, 6115–6135 (1970).
21. B. C. Edgar, "The structure of the magnetosphere as deduced from magnetospherically reflected whistlers," thesis, Stanford University, Stanford, CA (1972).
22. B. Á. Pataki, J. Lichtenberger, M. Clilverd, G. Máthé, P. Steinbach, S. Pásztor, L. Murár-Juhász, D. Koronczay, O. Ferencz, I. Csabai, Monitoring space weather: Using automated, accurate neural network based whistler segmentation for whistler inversion. *Space Weather* **20**, e2021SW002981 (2022).
23. B. C. Edgar, The upper- and lower-frequency cutoffs of magnetospherically reflected whistlers. *J. Geophys. Res.* **81**, 205–211 (1976).
24. J. Bortnik, U. S. Inan, T. F. Bell, Frequency-time spectra of magnetospherically reflecting whistlers in the plasmasphere. *J. Geophys. Res.* **108**, 1030 (2003).
25. I. Kimura, Effects of ions on whistler-mode ray tracing. *Radio Sci.* **1**, 269–284 (1966).
26. R. Raghuram, A new interpretation of subprotonospheric whistler characteristics. *J. Geophys. Res.* **80**, 4729–4731 (1975).
27. J. Chum, O. Santolik, M. Parrot, Analysis of subprotonospheric whistlers observed by DEMETER: A case study. *J. Geophys. Res.* **114**, A02307 (2009).
28. V. S. Sonwalkar, A. Reddy, Specularly reflected (SR) whistlers, paper presented at the *AGU Fall Meeting*, New Orleans, LA, 13 to 17 December 2021, abstract SM43C-02.
29. R. M. Thorne, R. B. Horne, Landau damping of magnetospherically reflected whistlers. *J. Geophys. Res.* **99**, 17249–17258 (1994).
30. J. M. Stratton, R. J. Harvey, G. A. Heyler, Mission overview for the radiation belt storm probes mission. *Space Sci. Rev.* **179**, 29–57 (2013).

31. C. A. Kletzing, W. S. Kurth, M. Acuna, R. J. MacDowall, R. B. Torbert, T. Averkamp, D. Bodet, S. R. Bounds, M. Chutter, J. Connerney, D. Crawford, J. S. Dolan, R. Dvorsky, G. B. Hospodarsky, J. Howard, V. Jordanova, R. A. Johnson, D. L. Kirchner, B. Mokrzycki, G. Needell, J. Odom, D. Mark, R. Pfaff Jr., J. R. Phillips, C. W. Piker, S. L. Remington, D. Rowland, O. Santolik, R. Schnurr, D. Sheppard, C. W. Smith, R. M. Thorne, J. Tyler, The Electric and Magnetic Field Instrument Suite and Integrated Science (EMFISIS) on RBSP. *Space Sci. Rev.* **179**, 127–181 (2013).
32. C. A. Kletzing, J. Bortnik, G. Hospodarsky, W. S. Kurth, O. Santolik, C. W. Smitth, I. W. Christopher, D. P. Hartley, I. Kolmasova, A. Sen Gupta, The Electric and Magnetic Fields Instrument Suite and Integrated Science (EMFISIS): Science, data, and usage best practices. *Space Sci. Rev.* **219**, 28 (2023).
33. R. M. Thorne, Unducted whistler evidence for a secondary peak in the electron energy spectrum near 10 keV. *J. Geophys. Res.* **73**, 4895–4904 (1968).
34. V. Sonwalkar, A. Reddy, J. Butler, A new interpretation of the upper- and lower-frequency cutoffs of lightning generated nonducted magnetospherically reflected (MR) whistlers: Remote sensing of magnetospheric plasma density and composition, paper presented at the *42nd COSPAR Scientific Assembly*, Pasadena, CA, 14 to 22 July 2018, abstract C5.1-52-18.
35. C. J. Rodger, S. Werner, J. B. Brundell, E. H. Lay, N. R. Thomson, R. H. Holzworth, R. L. Dowden, Detection efficiency of the VLF World-Wide Lightning Location Network (WWLLN): Initial case study. *Ann. Geophys.* **24**, 3197–3214 (2006).
36. J. D. Means, Use of the three-dimensional covariance matrix in analyzing the polarization properties of plane waves. *J. Geophys. Res.* **77**, 5551–5559 (1972).
37. M. L. Hutchins, R. H. Holzworth, J. B. Brundell, C. J. Rodger, Relative detection efficiency of the World Wide Lightning Location Network. *Radio Sci.* **47**, RS6005 (2012).
38. A. Reddy, V. S. Sonwalkar, Occurrence patterns of magnetospherically reflected (MR) and specularly reflected (SR) whistlers observed on Van Allen Probes, paper presented at the *AGU Fall Meeting*, San Francisco, CA, 22 January 2024, abstract SM01-05.
39. R. E. Orville, D., W. Spencer, Global lightning flash frequency. *Mon. Weather Rev.* **107**, 934–943 (1979).
40. R. H. Holzworth, J. B. Brundell, M. P. McCarthy, A. R. Jacobson, C. J. Rodger, T. S. Anderson, Lightning in the Arctic. *Geophys. Res. Lett.* **48**, e2020GL091366 (2021).
41. R. E. Orville, Peak-current variations of lightning return strokes as a function of latitude. *Nature* **343**, 149–151 (1990).
42. V. Cooray, M. Rubinstein, F. Rachidi, Latitude and topographical dependence of lightning return stroke peak current in natural and tower-initiated negative ground flashes. *Atmosphere* **11**, 560 (2020).
43. H. G. James, Refraction of whistler-mode waves by large-scale gradients in the middle-latitude ionosphere. *Ann. Geophys.* **28**, 301–339 (1972).
44. V. S. Sonwalkar, T. F. Bell, R. A. Helliwell, U. S. Inan, Direct multiple path magnetospheric propagation: A fundamental property of nonducted VLF waves. *J. Geophys. Res.* **89**, 2823–2830 (1984).
45. O. Santolík, M. Parrot, F. Lefeuvre, Singular value decomposition methods for wave propagation analysis. *Radio Sci.* **38**, 1010 (2003).
46. V. S. Sonwalkar, A. Reddy, D. L. Carpenter, Magnetospherically reflected, specularly reflected, and backscattered whistler mode radio sounder echoes observed on the IMAGE satellite: 2. Sounding of electron density, ion effective mass (m_{eff}), ion composition (H^+, He^+, O^+), and density irregularities along the geomagnetic field line. *J. Geophys. Res.* **116**, A11211 (2011).
47. V. S. Sonwalkar, A. Reddy, Plasmasphere tomography, paper presented at the *AGU Fall Meeting*, Chicago, IL, 12 to 16 December 2022), abstract SM54B-02.
48. R. A. Challinor, The phase velocity and attenuation of audio-frequency electro-magnetic waves from simultaneous observations of atmospherics at two spaced stations. *J. Atmos. Terr. Phys.* **29**, 803–810 (1967).
49. K. L. Graf, N. G. Lehtinen, M. Spasojevic, M. B. Cohen, R. A. Marshall, U. S. Inan, Analysis of experimentally validated trans-ionospheric attenuation estimates of VLF signals. *J. Geophys. Res. Space Phys.* **118**, 2708–2720 (2013).
50. R. Said, M. Gołkowski, V. Harid, Empirical parameterization of broadband VLF attenuation in the Earth-ionosphere waveguide. *J. Geophys. Res.* **128**, e2022JA030742 (2023).
51. M. Hanzelka, O. Santolik, M. Hajoš, F. Nemec, M. Parrot, Observation of ionospherically reflected quasiperiodic emissions by the DEMETER spacecraft. *Geophys. Res. Lett.* **44**, 8721–8729 (2017).
52. V. S. Sonwalkar, A. Reddy, A new interpretation of Nu whistlers observed on the OGO-1 satellite: Nu specularly reflected (SR) whistlers, paper presented at the *AGU Fall Meeting*, San Francisco, CA, 22 January 2024), abstract SM01-04.
53. U. S. Inan, T. F. Bell, The plasmapause as a VLF wave guide. *J. Geophys. Res.* **82**, 2819–2827 (1977).
54. J. L. Ristić-Djurović, T. F. Bell, U. S. Inan, Precipitation of radiation belt electrons by magnetospherically reflected whistlers. *J. Geophys. Res.* **103**, 9249–9260 (1998).
55. V. S. Sonwalkar, U. S. Inan, T. F. Bell, R. A. Helliwell, V. M. Chmyrev, Y. P. Sobolev, O. Y. Ovcharenko, V. Selegej, Simultaneous observations of VLF ground transmitter signals on the DE 1 and COSMOS 1809 satellites: Detection of a magnetospheric caustic and a duct. *J. Geophys. Res.* **99**, 17511–17522 (1994).
56. N. H. Dantas, "OGO-4 Satellite observations of whistler-mode propagation effects associated with countries in the magnetosphere" (Tech. Rep. 3469-1, Stanford Univ., 1972).
57. V. S. Sonwalkar, D. L. Carpenter, A. Reddy, R. Proddaturi, S. Hazra, K. Mayank, B. W. Reinisch, Magnetospherically reflected, specularly reflected, and backscattered whistler mode radio-sounder echoes observed on the IMAGE satellite: 1. Observations and interpretation. *J. Geophys. Res.* **116**, A11210 (2011).
58. R. R. Scarabucci, Satellite observations of equatorial phenomena and defocusing of VLF electromagnetic waves. *J. Geophys. Res.* **75**, 69–84 (1970).
59. V. S. Sonwalkar, J. Harikumar, An explanation of ground observations of auroral hiss: Role of density depletions and meter-scale irregularities. *J. Geophys. Res.* **105**, 18867–18883 (2000).
60. D. I. Golden, M. Spasojevic, F. R. Foust, N. G. Lehtinen, N. P. Meredith, U. S. Inan, Role of the plasmapause in dictating the ground accessibility of ELF/VLF chorus. *J. Geophys. Res.* **115**, A11211 (2010).
61. A. K. Singh, S. B. Singh, R. Singh, S. A. Gokani, A. K. Singh, D. Singh, J. Lichtenberger, Whistlers detected and analyzed by Automatic Whistler Detector (AWD) at low latitude Indian stations. *J. Atmos. Sol. Terr. Phys.* **121**, 221–228 (2014).
62. D. L. Carpenter, R. R. Anderson, An ISEE/whistler model of equatorial electron density in the magnetosphere. *J. Geophys. Res.* **97**, 1097–1108 (1992).
63. W. S. Kurth, S. De Pascuale, J. B. Faden, C. A. Kletzing, G. B. Hospodarsky, S. Thaller, J. R. Wygant, Electron densities inferred from plasma wave spectra obtained by the Waves instrument on Van Allen Probes. *J. Geophys. Res.* **120**, 904–914 (2015).
64. J. R. Wygant, J. W. Bonnell, K. Goetz, R. E. Ergun, F. S. Mozer, S. D. Bale, M. Ludlam, P. Turin, P. R. Harvey, R. Hochmann, K. Harps, G. Dalton, J. McCauley, W. Rachelson, D. Gordon, B. Donakowski, C. Shultz, C. Smith, M. Diaz-Aguado, J. Fischer, S. Heavner, P. Berg, D. M. Malsapina, M. K. Bolton, M. Hudson, R. J. Strangeway, D. N. Baker, X. Li, J. Albert, J. C. Foster, C. C. Chaston, I. Mann, E. Donovan, C. M. Cully, C. A. Cattell, V. Krasnoselskikh, K. Kersten, A. Brenneman, J. B. Tao, The electric field and waves instruments on the radiation belt storm probes mission. *Space Sci. Rev.* **179**, 183–220 (2013).
65. H. Zheng, R. H. Holzworth, J. B. Brundell, A. R. Jacobson, J. R. Wygant, G. B. Hospodarsky, F. S. Mozer, J. Bonnell, A statistical study of whistler waves observed by Van Allen Probes (RBSP) and lightning detected by WWLLN. *J. Geophys. Res. Space Phys.* **121**, 2067–2079 (2016).
66. G. B. Hospodarsky, W. S. Kurth, C. A. Kletzing, S. R. Bounds, O. Santolík, R. M. Thorne, W. Li, T. F. Averkamp, J. R. Wygant, J. W. Bonnell, "Plasma wave measurements from the Van Allen Probes" in *Magnetosphere-Ionosphere Coupling in the Solar System*, C. R. Chappell, R. W. Schunk, P. M. Banks, J. L. Burch, R. M. Thorne, Eds. (Wiley, 2016), pp. 127–143.
67. R. L. Dowden, J. B. Brundell, C. J. Rodger, VLF lightning location by time of group arrival (TOGA) at multiple sites. *J. Atmos. Sol. Terr. Phys.* **64**, 817–830 (2002).
68. C. J. Rodger, J. B. Brundell, R. H. Holzworth, E. H. Lay, Growing detection efficiency of the World Wide Lightning Location Network. *AIP Conf. Proc.* **1118**, 15–20 (2009).
69. J. Haselgrove, Ray theory and a new method for ray tracing, paper presented at the *Conference on the Physics of the Ionosphere*, Cambridge, London, January 1955, pp. 355–364.
70. K. G. Budden, *The Propagation of Radio Waves* (Cambridge Univ. Press, 1985).
71. M. C. Kelley, K. D. Baker, J. C. Ulwick, C. L. Rino, M. J. Baron, Simultaneous rocket probe, scintillation, and incoherent scatter radar observations of irregularities in the auroral zone ionosphere. *Radio Sci.* **15**, 491–505 (1980).
72. J. F. Vickrey, C. L. Rino, T. A. Potemra, Chatanika/Triad observations of unstable ionization enhancements in the auroral F-region. *Geophys. Res. Lett.* **7**, 789–792 (1980).
73. O. Santolík, M. Parrot, U. S. Inan, D. Burešová, D. A. Gurnett, J. Chum, Propagation of unducted whistlers from their source lightning: A case study. *J. Geophys. Res.* **114**, A03212 (2009).
74. U. S. Inan, T. F. Bell, R. R. Anderson, Cold plasma diagnostics using satellite measurements of VLF signals from ground transmitters. *J. Geophys. Res.* **82**, 1167–1176 (1977).
75. V. S. Sonwalkar, D. L. Carpenter, R. A. Helliwell, M. Walt, U. S. Inan, D. L. Caudle, M. Ikeda, Properties of the magnetospheric hot plasma distribution deduced from whistler mode wave injection at 2400 Hz: Ground-based detection of azimuthal structure in magnetospheric hot plasmas. *J. Geophys. Res.* **102**, 14363–14380 (1997).
76. J. H. Crary, "The effect of the Earth-ionosphere waveguide on whistlers" (Tech. Rep. 9, Stanford Univ., 1961).
77. E. L. Maxwell, Atmospheric noise from 20 Hz to 30 kHz. *Radio Sci.* **2**, 637–644 (1967).
78. K. Tsuruda, S. Machida, T. Terasawa, A. Nishida, K. Maezawa, High spatial attenuation of the Siple transmitter signal and natural VLF chorus observed at ground-based chain stations near Roberval, Quebec. *J. Geophys. Res.* **87**, 742–750 (1982).
79. V. Rakov, A. A. Dulzon, On latitudinal features of thunderstorm activity. *Meteor. Gidrol.* **1**, 52–57 (1984).
80. V. Rakov, A. A. Dulzon, Lightning research in Western Siberia, in *Proceedings of the 8th International Conference on Atmospheric Electricity* (Institute of High Voltage Research, 1988), pp. 766–769.
81. O. Pinto Jr., I. R. C. A. Pinto, M. Lacerda, A. M. Carvalho, J. H. Diniz, L. C. L. Cherchiglia, Are equatorial negative lightning flashes more intense than those at higher latitudes? *J. Atmos. Sol. Terr. Phys.* **59**, 1881–1883 (1997).

82. S. Visacro, C. R. Mesquita, A. De Conti, F. H. Silveira, Updated statistics of lightning currents measured at Morro do Cachimbo station. *Atmos. Res.* **117**, 55–63 (2012).
83. T. F. Bell, The nonlinear gyroresonance interaction between energetic electrons and coherent VLF waves propagating at an arbitrary angle with respect to the Earth's magnetic field. *J. Geophys. Res.* **89**, 905–918 (1984).
84. A. B. Carlson, P. B. Crilly, *Communication Systems* (McGraw Hill, ed. 5, 2010).

Acknowledgments: We gratefully acknowledge the assistance of W. S. Kurth, G. B. Hospodarsky, and J. Faden for help with access to Van Allen Probes EMFISIS data and software. We wish to thank the WWLLN (http://wwlln.net), a collaboration among over 50 universities and institutions, for providing the lightning location data used here. In particular, we thank R. H. Holzworth for help with access to WWLLN lightning data and for providing lightning data used here. We thank M. Cohen and R. Moore for useful discussions. **Funding:** This work was supported by the National Science Foundation grant 2015765 (V.S.S. and A.R.) and National Aeronautics and Space Administration grant 80NSSC23M0070 (A.R. and V.S.S.). **Author contributions:** V.S.S. led the conceptual organization, interpretation, writing, development of the propagation model, provided supervision, and assisted in other aspects of the paper. A.R. led the ray tracing simulations, data analysis, visualization, numerical implementation of the propagation model, and assisted in other aspects of the paper. **Competing interests:** The authors declare that they have no competing interests. **Data and materials availability:** All data needed to evaluate the conclusions in the paper are present in the paper and/or the Supplementary Materials. Van Allen Probes data are publicly available (https://emfisis.physics.uiowa.edu/data/index). WWLLN data used here are given in the main text and supplementary figures and tables and were provided to the authors free of charge. The WWLLN archival data are copyrighted by the University of Washington and are available at a nominal cost. Please contact R. Holzworth (email: bobholz@washington.edu). A Stanford ray tracer code is available at https://github.com/asousa/Stanford_Raytracer.

Submitted 24 January 2024
Accepted 11 July 2024
Published 16 August 2024
10.1126/sciadv.ado2657